Scheme for the Balance Between Stability and Maneuverability of Hypersonic Vehicle

Wu Yushan, *Jiang Ju* *, *Zhen Ziyang*, *Jiao Xin*, *Gu Chenfeng*

College of Automation Engineering, Nanjing University of Aeronautics and Astronautics, Nanjing 210016, P. R. China

(Received 4 May 2015; revised 1 January 2016; accepted 21 February 2016)

Abstract: Since the aerodynamic center moving backward sharply in hypersonic flight, the stability margin of the hypersonic vehicle increases largely while the maneuverability decreases. We proposed a novel method to solve this contradiction. We used relaxed static stability (RSS) to improve the maneuverability in hypersonic flight, and designed the stability augmentation system (SAS) to ensure the stability in subsonic flight. Therefore, the relationship between static stability and maneuverability was quantitatively analyzed in the first step, and the numerical value of RSS was obtained on the premise of good maneuverability. Secondly, the relationship between static stability and aerodynamic parameters was quantitatively analyzed. We properly adjusted aerodynamic parameters based on the quantitative relationship to achieve the specific static stability set in the first step, and therefore provided the engineering realization methods. The vehicle will be statically unstable in subsonic flight with the specific static stability. Lastly, SAS was needed to ensure the stability of the vehicle in subsonic flight. Simulation studies were conducted by comparing the linear SAS to the nonlinear SAS, and the results showed that the nonlinear dynamic-inversion controller can synthesize with proportional-integrall-derivative(PID) controller robustly and stabilize the hypersonic vehicle.

Key words: hypersonic vehicle; relaxed static stability; stability augmentation system; dynamic inversion control; conventional feedback control

CLC number: V249 **Document code**: A **Article ID**: 1005-1120(2017)06-0647-12

0 Introduction

A hypersonic vehicle generally refers to a vehicle flying at Mach 5 or above[1]. As a promising space vehicle to achieve fast global response, hypersonic vehicles have attracted increasing commercial and military interests[2-6]. Despite several advantages, it also brings many challenges and a vast amount of tasks still to be solved[7].

When the speed of a hypersonic vehicle increases from subsonic to hypersonic range, the aerodynamic center of the vehicle will move sharply backward, which largely improves the stability margin while decreasing the maneuverability. Therefore, the contradiction between stability and maneuverability needs to be solved urgently. Relaxed static stability (RSS) is regarded as a general way to solve it[8-10].

However, RSS is seldom quantitatively studied for hypersonic vehicles at present. For a good maneuverability in hypersonic flight, hypersonic vehicles are quantitatively designed to be statically unstable in subsonic flight with RSS. Therefore, they are is less stable and more maneuverable in hypersonic flight than general vehicles. Consequently, a stability augmentation system (SAS) is needed to ensure the stability of the statically unstable vehicle in subsonic flight.

Linear control methods have been applied to the SAS design of most modern airliners[9,11], including the conventional feedback control and the optimal control. The pitch rate and the normal overload were fed back synthetically to the elevator channel in the augmentation control system by Chen Chuang[12]. LQR was applied to modern airliners with RSS by Blight[13]. Sum of squares

* Corresponding author, E-mail address: jiangju@nuaa.edu.cn.

How to cite this article: Wu Yushan, Jiang Ju, Zhen Ziyang, et al. Scheme for the balance between stability and maneuverability of hypersonic vehicle[J]. Trans. Nanjing Univ. Aero. Astro., 2017, 34(6): 647-658.
http://dx.doi.org/10.16356/j.1005-1120.2017.06.647

optimization was used to analyze the aircraft pitch axis SAS[14]. However, the linear SAS has its limits[15]. Linear control method is used by linearizing the model at a given operating point, but if the system dynamics are highly nonlinear or the system deviates significantly from the operating point, the linear SAS may not work effectively.

Nonlinear control methods have also been applied to the SAS design of some other aircraft. The thrust vector was combined with the dynamic-inversion by Steinhauser[16] to analyze the impact of RSS on lateral flying qualities of X-31A. The multi-objective design of a fuzzy logic augmented flight controller for a high performance fighter jet was described by Stewart[17].

The basic idea of dynamic inversion control is to cancel the nonlinear dynamics of nonlinear system by using feedback function, then, the unsatisfied dynamics will be replaced by the desired linear ones[18]. When dealing with the control problem of nonlinear system with multi-input and multi-variable, dynamic inversion control method can simplify the design process dramatically. Nevertheless, the dynamic inversion method is much more sensitive to the modeling errors. This method will present a bad performance in the presence of modeling uncertainties. Experts proposed several ways to improve the robustness of this method among which proportional integral derivative(PID) was the easiest way for engineering realization[19-24]. PID has attracted significant interests in aircraft control areas, thanks to its simple design process and strong robustness against external disturbances and parameter variations. Therefore, we combined PID with the dynamic inversion method to improve the robustness in this paper.

How to quantitatively solve the contradiction between stability and maneuverability of hypersonic vehicles has seldom been studied and the study of SAS on hypersonic vehicles is rare either. We proposed a novel way to solve the contradiction quantitatively and also presented a relaxation process.

1 Hypersonic Vehicle Model

The research object is a hypersonic vehicle with variable winglets on both sides of the fixed-wing. The function of the winglets is to increase the lift as well as the flight efficiency. Stretching and retracting winglets can also effectively change the aerodynamic parameters in order to achieve the specific static stability.

Our model is comprised of five state variables $\boldsymbol{X}=[V,h,\alpha,\gamma,q]^{\mathrm{T}}$ and two control inputs $\boldsymbol{U}_c=[\delta_e,\mathrm{PLA}]^{\mathrm{T}}$, where V is the velocity, γ the flight path angle, h the altitude, α the attack angle, q the pitch rate, δ_e the elevator deflection and PLA the throttle setting. The fifth-order longitudinal equations of the hypersonic vehicle are, respectively[25-26]

$$\begin{aligned}\dot{V}&=\frac{T\cos\alpha-D}{m}-g\times\sin\gamma\\ \dot{\gamma}&=\frac{L+T\sin\alpha}{mV}-\frac{g\times\cos\gamma}{V}\\ \dot{h}&=V\sin\gamma\\ \dot{\alpha}&=q-\dot{\gamma}\\ \dot{q}&=M_{yy}/I_{yy}\end{aligned}\tag{1}$$

The value of the lift, the drag, the pitching moment and the radius from the Earth's center are modeled, respectively, as[27]

$$\begin{aligned}L&=0.5\rho V^2sC_L\\ D&=0.5\rho V^2sC_D\\ M_{yy}&=0.5\rho V^2sc[C_M(\alpha)+C_M(\delta_e)+C_M(q)]\\ r&=h+R_E\end{aligned}\tag{2}$$

Different phases of thrust are modeled, respectively, as[28]

$$\begin{aligned}T=&\ \mathrm{PLA}\cdot(2.99\times10^5-h+1.33\times10^{-4}h^2-\\ &6.48\times10^{-10}h^3+3.75\times10^3\cdot Ma^3,0\leqslant Ma\leqslant2\\ &2\leqslant Ma\leqslant6\\ T=&\ \mathrm{PLA}\cdot(7.53\times10^2\cdot Ma^7-1.50\times10^4\cdot Ma^6+\\ &1.16\times10^5\cdot Ma^5-4.36\times10^5\cdot Ma^4+\\ &8.07\times10^5\cdot Ma^3-6.97\times10^5\cdot Ma^2+\\ &3.94\times10^5\cdot Ma+3.93\times10^{-8})\\ &2\leqslant Ma\leqslant6\end{aligned}\tag{3}$$

$$\begin{aligned}T=&-5.43\times10^4+6.64\times10^{-1}\times h+\\ &3.24\times10^5\times\mathrm{PLA}+3.74\times10^{-1}\times(h\times\mathrm{PLA})\\ &6\leqslant Ma\leqslant24;h<57\ 000\ \mathrm{ft}\\ T=&-1.64\times10^4+3.24\times10^5\times\mathrm{PLA}+\\ &3.24\times10^5\times\mathrm{PLA}+2.1295\times10^4\times\mathrm{PLA}\\ &h>57\ 000\ \mathrm{ft}\end{aligned}$$

Relationship between aerodynamic parameters and attack angles is formulated from the em-

pirical formula. In order to build an accurate model for control design in subsonic flight, the aerodynamic parameters are replaced with curve-fitted approximation based on the relationship and given points. The aerodynamic parameters of stretching winglets are used in taking off and climbing phase while the aerodynamic parameters of retracting winglets are used in hypersonic cruise. The fitting curves of stretching winglets at $Ma=0.8$ are shown in Figs. 1—3.

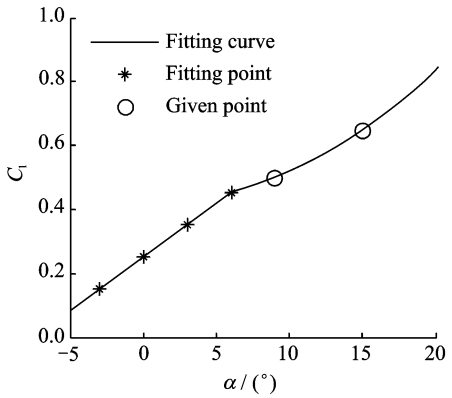

Fig. 1 Fitting curve of lift coefficient C_l at $Ma=0.8$

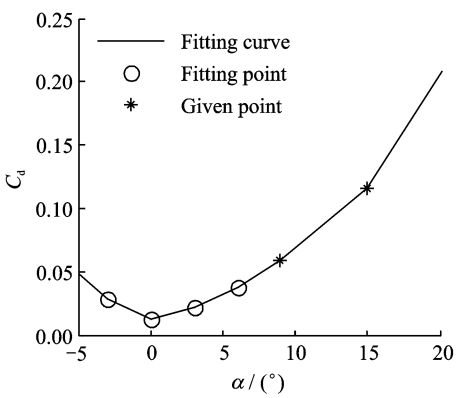

Fig. 2 Fitting curve of drag coefficient C_d at $Ma=0.8$

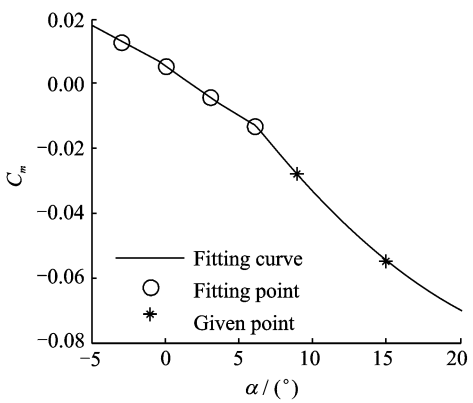

Fig. 3 Fitting curve of pitching moment coefficient C_m at $Ma=0.8$

The parameter perturbations of the hypersonic vehicle is defined as

$$\begin{aligned} m &= m_0(1+\Delta m)\\ I_{yy} &= I_0(1+\Delta I)\\ s &= s_0(1+\Delta s)\\ c &= c_0(1+\Delta c) \end{aligned} \tag{4}$$

2 Quantitative Relationship Between Static Stability and Maneuverability

In this section, the quantitative relationship between static stability and maneuverability is firstly studied. In terms of the studied relationship, we can obtain the specific static stability on the premise of good maneuverability. In addition, a way to relax the hypersonic vehicle to the specific static stability is proposed.

2.1 Relationship between static stability and maneuverability

From the longitudinal, we obtain

$$\dot{\gamma}=\frac{L+T\sin\alpha}{mV}-\frac{g\times\cos\gamma}{V} \tag{5}$$

Multiply mV at both sides, we can get

$$mV\dot{\gamma}=L+T\sin\alpha-mg\cos\gamma \tag{6}$$

$N_f=L+T\sin\alpha$ represents the normal force without gravity. Next, dividing mg at both sides, we can obtain

$$\frac{V}{g}\dot{r}=n-\cos\gamma \tag{7}$$

where n is the normal overload, $n=\frac{N_f}{mg}$. Thus,

$$n=\frac{V}{g}\dot{\gamma}+\cos\gamma \tag{8}$$

In terms of linearization, the deviation expression is written as

$$\Delta n_Z=\frac{\Delta V}{g}\frac{\mathrm{d}\gamma_0}{\mathrm{d}t}+\frac{V_0}{g}\frac{\mathrm{d}\Delta\gamma}{\mathrm{d}t}-\Delta\gamma\sin\gamma_0 \tag{9}$$

The quadratic differential $\Delta\gamma\sin\gamma_0$ and the deviation ΔV are neglected for the sake of brevity, therefore

$$n\approx\frac{V}{g}\frac{\mathrm{d}\gamma}{\mathrm{d}t} \tag{10}$$

According to the small-perturbation theory in Ref. [29], the standard expressions of linear small-perturbation are derived by using the dy-

namic coefficients. The standard expressions are defined as follows

$$\begin{gathered}\Delta\dot{V}+a_{11}\Delta V+a_{14}\Delta\alpha+a_{13}\Delta\gamma=0\\ \Delta\ddot{\theta}+a_{21}\Delta V+a_{22}\Delta\dot{\theta}+a_{24}\Delta\alpha+a'_{24}\Delta\dot{\alpha}=\\ -a_{25}\Delta\delta_e-a'_{25}\Delta\dot{\delta}_e\\ \Delta\dot{\gamma}+a_{31}\Delta V+a_{33}\Delta\gamma-a_{34}\Delta\alpha=a_{35}\Delta\delta_e\\ \Delta\theta=\Delta\gamma+\Delta\alpha\end{gathered}\tag{11}$$

where $a_{22}=-\dfrac{M_q}{I_{yy}}, a_{24}=-\dfrac{M_\alpha}{I_{yy}}, a_{25}=-\dfrac{M_{\delta_e}}{I_{yy}}, a_{21}=-\dfrac{M_V}{I_{yy}}$, $a_{24}=-\dfrac{M_\alpha}{I_{yy}}$, $a_{25}=-\dfrac{M_{\delta_e}}{I_{yy}}$, $a_{34}=-\dfrac{(T+L_\alpha)}{mV}$, $a_{35}=\dfrac{L_{\delta_e}}{mV}$, $a_{33}=-\left(\dfrac{g}{V}\sin\gamma\right)$, $a_{31}=-\dfrac{(T_V\alpha+L_V)}{mV}$, $a_{14}=\dfrac{(T\alpha+D_a)}{m_0}$, $a_{13}=(g\cos\gamma)_0$, $a_{11}=-\dfrac{(T_V-X_V)}{m_0}$.

The maneuverability can be measured by the maximum normal overload of the vehicle. For the calculation of the maximum normal overload, the normal overload produced by unit deflection of the elevator should firstly be calculated. The transfer function from the normal overload n in Eq. (10) to the elevator deflection δ_e is defined

$$W_{\delta n}(s)=-\frac{\Delta n(s)}{\Delta\delta_e(s)}=-\frac{s\Delta\gamma(s)}{\Delta\delta_e}\frac{V}{g}=\frac{V}{g}sW_{\delta\gamma}(s)\tag{12}$$

Cramer rules are used to obtain

$$W_{\delta\gamma}(s)=\frac{K_\alpha}{s(T_\alpha^2s^2+2\xi_\alpha T_\alpha s+1)}\tag{13}$$

where $K_\alpha=\dfrac{a_{25}a_{34}-a_{24}a_{35}}{a_{24}+a_{22}a_{34}}, T_\alpha=\dfrac{1}{\sqrt{a_{24}+a_{22}a_{34}}}s$, $\xi_\alpha=\dfrac{a_{22}+a_{22}a_{24}}{2\sqrt{a_{24}+a_{22}a_{34}}}$.

In Eq. (12), $W_{\delta\gamma}(s)$ is substituted as

$$W_{\delta n}(s)=\frac{V}{g}\frac{K_\alpha}{(T_\alpha^2s^2+2\xi_\alpha T_\alpha s+1)}\tag{14}$$

According to Eq. (13), the physical meaning of K_α is the proportion of the steady value of $\Delta\gamma$ to the elevator deflection δ_e at the end of transient process. Therefore, the measurement index of maneuverability can be defined as the proportion of the normal overload to unit elevator deflection at the end of transient process, it can be written as

$$W_{(\delta n)w}=\frac{V}{g}K_\alpha=\frac{V}{g}\frac{a_{25}a_{34}-a_{24}a_{35}}{a_{24}+a_{22}a_{34}}\tag{15}$$

We remove a_{22}, a_{35} because of their tiny values, thus

$$W_{(\delta n)w}\approx\frac{V}{g}\frac{a_{25}a_{34}}{a_{24}+a_{22}a_{34}}=\frac{V}{g}\left(\frac{M_{\delta_e}\dfrac{T+L_\alpha}{mV}}{M_\alpha+M_q\dfrac{T+L_\alpha}{mV}}\right)=\frac{V}{g}\left(\frac{C_{m\delta_e}QSc\dfrac{T+C_{L_\alpha}QS}{mV}}{-C_{L_\alpha}SmQSc+C_{mq}QSc\dfrac{T+C_{L_\alpha}QS}{mV}}\right)\tag{16}$$

where Q represents the dynamic pressure $Q=\dfrac{1}{2}\rho V^2$, S the wing reference area, c the wing mean geometric chord, and S_m the static stability, where

$$S_m=\bar{x}_{ac}-\bar{x}_{cg}=\frac{x_{ac}}{c}-\frac{x_{cg}}{c}\tag{17}$$

where x_{ac} represents the position of the aerodynamic center and x_{cg} the position of the gravity center.

The position of the gravity center is moved to achieve RSS. The effects of changing static stability S_m on the aerodynamic parameters are discussed, respectively,

(1) The change of S_m has no influence on C_{L_α}, C_L, C_D by moving the position of the gravity center.

$$(2)\ C_{m\delta_e}=-C_{L_{\delta_e}}\frac{L_{pw}}{c}=-C_{L_{\delta_e}}\frac{x_{pw}-x_g}{c}=-C_{L_{\delta_e}}\frac{x_{pw}-(x_f-S_m\cdot c)}{c}\tag{18}$$

$$(3)\ C_{mq}=-2C_{L_{pw}}\cdot\frac{S_{pw}}{S}(\bar{x}_{pw}-\bar{x}_g)^2\sqrt{k}\tag{19}$$

$$(4)\ C_{m_\alpha}=C_{L_\alpha}(\bar{X}_g-\bar{X}_f)\tag{20}$$

Substitute Eqs. (18), (19) in to Eq. (16), the simulation result on the unit normal overload with S_m is obtained in Fig. 4.

The maneuverability index (the maximum normal overload of the vehicle) is produced when the elevator deflects to the limited angle ($\pm20°$), therefore, the simulation result on varying maneuverability index with S_m is obtained in Fig. 5.

In order to ensure the good maneuverability in hypersonic flight, the measurement index of maneuverability should value between 2.5—7[30-31]. Maneuverability cannot be ensured

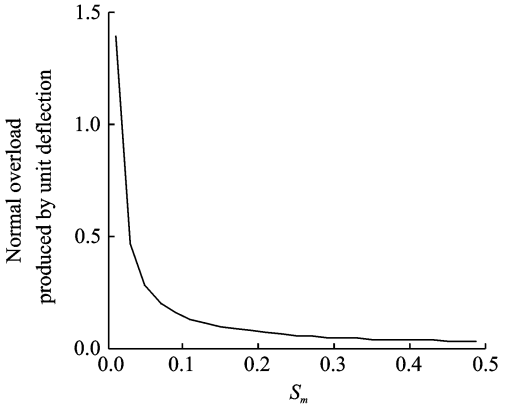

Fig. 4 Simulation results on unit normal overload with S_m

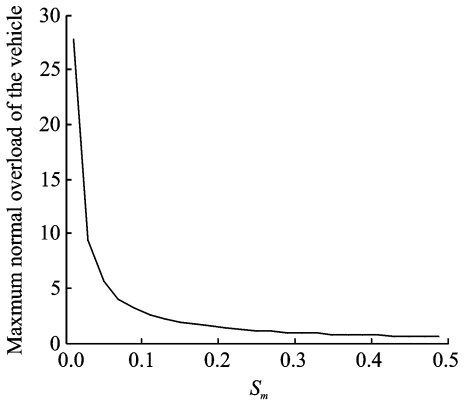

Fig. 5 Simulation results on varying maneuverability index with S_m

when the measurement index of maneuverability is under 2.5 and both the vehicle and the pilots can hardly bear if the measurement index of maneuverability is over 7.

Based on the original given position of the gravity center, the measurement index of maneuverability of the original vehicle is calculated to be 1.25, which is under the proper value interval of the measurement index. The process to obtain the numerical value of S_m on the premise of good maneuverability is as follows.

The calculated value of S_m in hypersonic flight should be between 0.04—0.11.

Position of the gravity center is derived as follows

$$X_g = X_f - S_m \cdot c \tag{21}$$

Hence, we know X_g is calculated between 21.8—23.2 m. The subsonic value of aerodynamic center coefficient is given to be 0.6, and the static stability formula is $S_m = (X_f - X_g)/c$. As a result, the calculated value of S_m in subsonic flight should be between −0.19——0.26.

2.2 The specific static stability

According to previous section, value of RSS should be between −0.14——0.26. Considering the effects of changing static stability S_m on the aerodynamic parameters discussed before and the formula $C_m = C_{m_0} + C_{m_\alpha}\alpha + C_{m\delta_e}\delta_e + C_{mq}q$, the simulation result is obtained in Fig. 6.

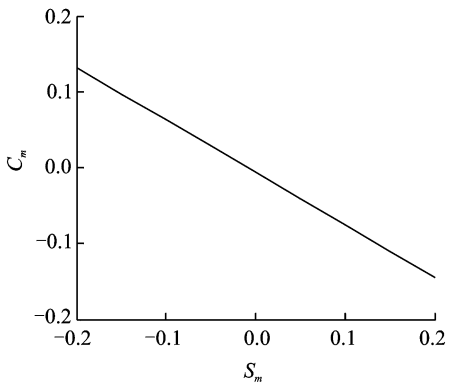

Fig. 6 Simulation result on varying pitching moment C_m with S_m

Fig. 6 illustrates that S_m decreases as C_m increases. Thus, in order to achieve the specific static stability, both the curve-fitted C_m and the derivative of the curve (C_{m_α}) are required to increase properly, as shown in Fig. 7 and Table 1.

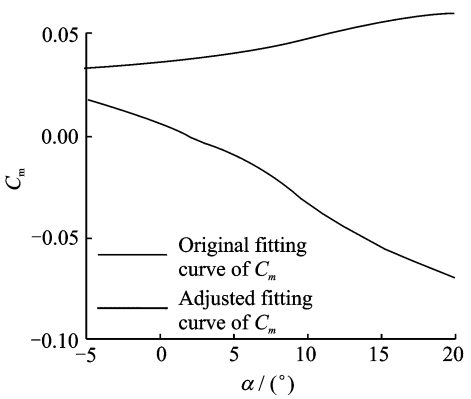

Fig . 7 Adjusted fitting curve of $C_m 1$ at $Ma = 0.8$

Table 2 shows several engineering realization ways to increase C_m, C_{m_α} and the possibility to use them in the hypersonic vehicle.

Now the proof is provided to show the cor-

rectness of the adjusted fitting interpolation of C_m.

The force diagram of the vehicle with RSS in subsonic flight is shown in Fig. 8.

The subsonic aerodynamic center coefficient is 0.6. We can get from Fig. 8 that

$$\begin{cases} L_f \cdot l_f = L_{pw} \cdot l_{pw} \\ l_f + l_{pw} = l_w - l_z \times 0.6 = 29 - 30 \times 0.6 = 11 \end{cases} \tag{22}$$

Table 1 The increased fitting interpolation of C_m

Ma	α/(°)												
	−30	−15	−3	0	3	6	9	15	30	45	60	75	90
0	0.031 7	0.039	0.040 8	0.042 8	0.047 8	0.055 9	0.065 9	0.075 9	0.091 9	0.100 5	0.12	0.127 1	0.150 7
0.3	0.026 4	0.031 7	0.033 5	0.035 5	0.038 5	0.041 6	0.045 6	0.055 6	0.061 6	0.070 2	0.079 7	0.086 8	0.100 4
0.5	0.025 1	0.030 4	0.032 2	0.034 2	0.037 2	0.040 3	0.043 3	0.048 3	0.054 3	0.062 9	0.072 4	0.079 5	0.093 1
0.8	0.019 8	0.025 1	0.026 9	0.027 9	0.028 9	0.03	0.031	0.036	0.042	0.050 6	0.060 1	0.067 2	0.080 8
2	0.018 1	0.015	0.012 7	0.012 2	0.011 6	0.011 1	0.010 5	0.009 3	0.006	0.002 4	−0.001	−0.005	−0.009
3	0.016 1	0.014 2	0.012 7	0.012 3	0.012	0.011 6	0.011 2	0.010 4	0.008 5	0.006 6	0.004 7	0.002 8	0.000 9
5	0.015 4	0.013 9	0.012 7	0.012 4	0.012 1	0.011 8	0.011 5	0.010 9	0.009 4	0.007 9	0.006 4	0.004 9	0.003 4
8	0.010 1	0.006	0.002 7	0.001 8	0.001 1	0.000 2	7E−04	−0.002	−0.007	−0.011	−0.016	−0.02	−0.024
12	0.017 3	0.003 6	−0.007	−0.01	−0.013	−0.016	−0.019	−0.025	−0.039	−0.054	−0.069	−0.084	−0.099
15	0.018 4	−0.007	−0.028	−0.033	−0.037	−0.043	−0.048	−0.059	−0.087	−0.114	−0.142	−0.169	−0.197
18	0.016 4	−0.025	−0.058	−0.066	−0.074	−0.082	−0.091	−0.109	−0.153	−0.198	−0.242	−0.287	−0.331
20	0.019	−0.035	−0.078	−0.089	−0.098	−0.11	−0.122	−0.145	−0.203	−0.261	−0.319	−0.377	−0.435
25	0.009	−0.084	−0.158	−0.177	−0.194	−0.214	−0.234	−0.274	−0.374	−0.474	−0.574	−0.675	−0.775

Table 2 Engineering realization ways to increase C_m, C_{m_a}

Engineering realization ways	Possibility to use in the hypersonic vehicle
Gravity center back-shift	Big: This is the easiest way. Adjusting the fuel tank position would work.
Retracting winglets	Big: Retracting winglets is the easiest way to move the dynamic center forward, which will increase ultimately.
Adding canard wings	Small: Adding canard wings will sharply increase the drag in hypersonic flight.
Increasing the aspect ratio	Small: Increasing the aspect ratio will increase the drag in hypersonic flight.

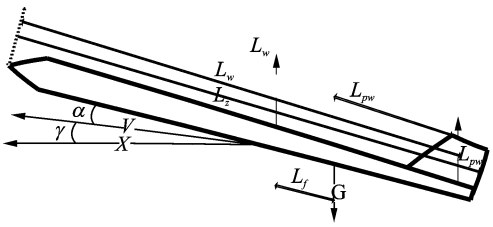

Fig. 8 Forces of the hypersonic vehicle in subsonic flight

where $L_f = \frac{1}{2}\rho V^2 S C_L = \frac{1}{2}\rho V^2 S C_{L_\alpha}\alpha$, $L_{pw} = \frac{1}{2}\rho V^2 S_{pw} C_{L_{pw}} = \frac{1}{2}\rho V^2 S_{pw} C_{L_{\delta_e}}\delta_e$.

A subsonic trim point of the new hypersonic vehicle model is obtained by using new C_m: $V=108$ m/s, $\alpha=4.81°$, $q=0°/s$, $\gamma=4.81°$, $\delta_e=8.41°$, $h=2\,009.38$ m. Hence, we can calculate that

$$l_f \approx 4.5, l_{pw} \approx 6.5$$

Consequently, the static stability is calculated as $S_m = \overline{X}_f - \overline{X}_g = (18-22.5)/20 = -0.225$, which is in the proper interval -0.19—-0.26. Therefore, the measurement index of maneuverability of the vehicle with specific RSS is calculated as 3.86, which is in the proper value interval 2.5—7. Ultimately, the correctness of the adjusted fitting interpolation of C_m is proved.

3 Stability Augmentation System for Hypersonic Vehicle With Relaxed Static Stability

3.1 Stability augmentation system design based on the conventional feedback control

3.1.1 Controller design

The conventional feedback control is commonly used in modern airliner. Severe nonlinearity, strong couplings, various uncertainties are big challenges for hypersonic fight control design,

because high velocity causes vehicle very sensitive to changes in flight condition. We verifiy the applicability of conventional feedback control method to hypersonic vehicle.

Short-period motion plays the leading role at the initial stage of the longitudinal motion. Long-period motion can be neglected. The pitch rate feedback control, the attack angle feedback control, the normal overload feedback control and the mixed comprehensive feedback control are included in the conventional feedback control methods. Combination of the attack angle feedback control and the pitch rate feedback control are used in this paper, which guarantees the control precision as well as the reliability. The new hypersonic vehicle model with adjusted increased C_m obtained in previous section is used in this section. The control law of the controller is as

$$\Delta\delta_e = K_q \Delta q + K_\alpha \Delta\alpha \tag{23}$$

where $c_1 = -\left(\frac{Z_\alpha}{V} + M_q + M_{\dot{\alpha}}\right)$, $c_2 = \frac{M_q Z_\alpha}{V} - M_\alpha$

Block diagram of the controller is shown in Fig. 9.

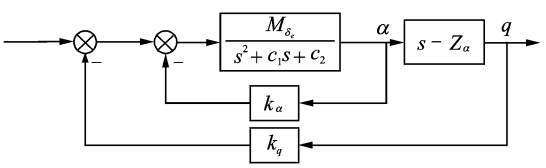

Fig. 9 Block diagram of the controller

The transfer function is obtained by substituting the adjusted aerodynamic parameters to the model. Then, we know

$$\frac{\Delta\alpha}{\Delta\delta_e} = \frac{0.369\ 9}{s^2 + 0.422\ 3s + (23.613\ 6 + 0.369\ 9k_\alpha)} \tag{24}$$

$$\frac{\Delta q}{\Delta\delta_e} = (0.369\ 9s + 0.156\ 2)/ \left[s^2 + (0.422\ 3 + 0.369\ 9k_q)s + 23.613\ 6 + 0.369\ 9k_\alpha + 0.156\ 2k_q\right] \tag{25}$$

After dividing the nonlinear vehicle model into two SISO linear systems, the root locus method is used to obtain the proper closed-loop gain which will basically improve the dynamic performance. Root locus method is used to find out k_α, k_q with best dynamic performance, consequently

$$k_\alpha = 3, k_q = 10$$

3.1.2 Simulation results

The controller designed based on the conventional feedback control is applied to the nonlinear vehicle model. The simulation results are shown in Figs. 10—12.

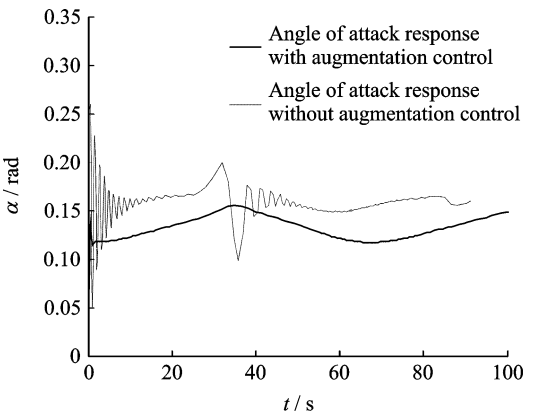

Fig. 10 Attack angle response

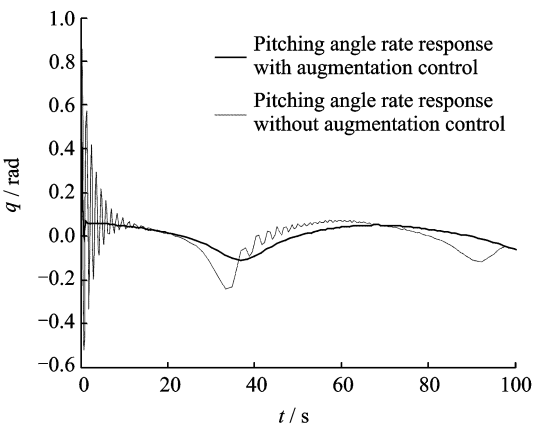

Fig. 11 Pitch rate response

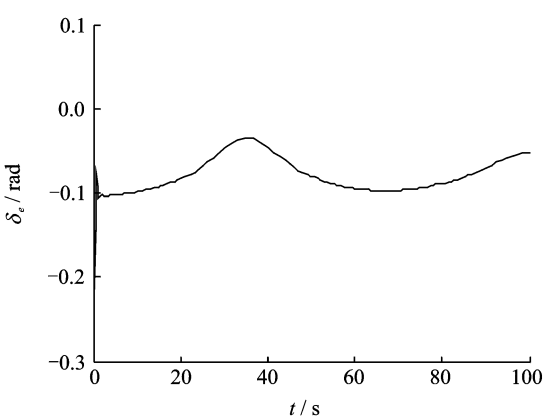

Fig. 12 Track angle response

From the results, conclusion is drawn that the linear SAS applied to the hypersonic vehicle with specific static stability is capable of improving the dynamic performance of the short-period motion, but the conventional feedback control method can not guarantee the dynamic performance in long-period motion because of the severe nonlinearity, strong couplings and various uncertainties of the hypersonic vehicle. Adjusting k_α, k_q is only capable of improving the dynamic performance of the short-period motion. As a result, a nonlinear control method with high control precision is needed.

3.2 Stability augmentation system design based on dynamic inversion-PID method

PID combined with the dynamic inversion method is applied to the hypersonic vehicle, and the simulation demonstrates the controller performance.

3.2.1 Feedback linearization

The adjusted increased C_m obtained in Section 2.1 is used to build the subsonic vehicle model. Elevator deflection δ_e is the system input while the attack angle α and the pitch rate q are the outputs. Feedback linearization is applied to obtain affine nonlinear equations, where state variables are $\boldsymbol{x}=[q\ \alpha]^{\mathrm{T}}$, control variable is $u=\delta_e$, outputs are $\boldsymbol{y}=[q\ \alpha]^{\mathrm{T}}$. The affine nonlinear equations are defined as

$$\begin{bmatrix}\dot{q}\\ \dot{\alpha}\end{bmatrix}=\begin{bmatrix}\dfrac{1}{I_{yy}}qS_c\bar{c}(C_{M\alpha}+C_{Mq}-C_e\alpha)\\ q-(\dfrac{1}{Mv})qS_c(C_L+C_T\sin\alpha)+\dfrac{g\sin\gamma}{\gamma}\end{bmatrix}+\begin{bmatrix}C_e\\ 0\end{bmatrix}\delta_e$$

$$\boldsymbol{y}=\begin{bmatrix}1 & 0\\ 0 & 1\end{bmatrix}\boldsymbol{x} \tag{26}$$

3.2.2 Controller design

The prerequisite to use the dynamic inversion is that the number of state variables is the same as the number of control variables. Therefore, the nonlinear system should be divided into several subsystems based on the respond speed, and the number of each subsystem's state variables should be the same as the number of control variables. Then, the dynamic inversion can be applied to each subsystem respectively.

The system can be divided into the fast subsystem and the slow subsystem based on the respond speed. The speed of pitch rate response is much faster than attack angle response. Therefore, the pitch rate subsystem is the fast subsystem while the attack angle subsystem is the slow subsystem.

(1)Controller design for fast subsystem

The fast subsystem is defined as

$$\dot{q}=A_1+Bu \tag{27}$$

where $A_1=\dfrac{1}{I_{yy}}qS_c\bar{c}(C_{M\alpha}+C_{Mq}-C_e\alpha)$, $B=C_e$, $u=\delta_e$. The dynamic inversion control law for the fast subsystem is given as

$$u=B^{-1}(v-A_1) \tag{28}$$

where $v=k_f(q_c-q)$, k_f is the bandwidth of the fast subsystem. The selected k_f is given as

$$k_f=10\ \mathrm{rad/s}$$

q_c is not only the command signal for the slow subsystem but also the steady value of the fast subsystem. The fast subsystem eventually becomes

$$\dot{q}=v \tag{29}$$

(2)Controller design for slow subsystem

The slow subsystem is the outer layer of the fast subsystem. The input of the slow subsystem is the command signal α_c produced by second-order system. The output of the slow subsystem is the input of fast subsystem q_c. The slow subsystem can be defined as

$$\dot{\alpha}=A_2+Au \tag{30}$$

where $A_2=-\left(\dfrac{1}{mv}\right)qS_c(C_L+C_T\sin\alpha)+\dfrac{g\sin\gamma}{v}$, $A=1$, $u=q$. The dynamic inversion control law for the slow subsystem is given as

$$u=A^{-1}(\dot{\alpha}_c-A_2) \tag{31}$$

where $\dot{\alpha}_c=k_d(\alpha_c-\alpha)$, k_d is the bandwidth of the slow subsystem. The selected k_d is given as

$$k_d=3\ \mathrm{rad/s}$$

The slow subsystem eventually becomes

$$\dot{\alpha}=\dot{\alpha}_c \tag{32}$$

The structure of dynamic-inversion controller for the hypersonic vehicle is shown in Fig. 13.

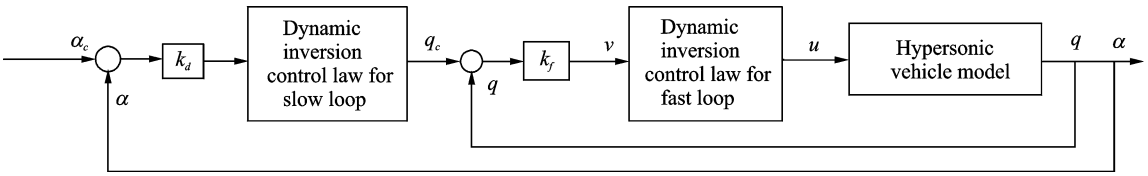

Fig. 13 Structure of dynamic-inversion controller for the hypersonic vehicle

(3)Dynamic-inversion PID controller design

From the previous controller design process, we know that accurate vehicle modeling is the premise condition for the good performance of the dynamic-inversion controller. Severe uncertainties of the hypersonic vehicle can cause big problems for the controller. Equation shows the uncertainties of the hypersonic vehicle.

To solve these problems, dynamic-inversion controller is combined with PID controller to eliminate the error as well as to increase the robustness. Slow subsystem is satisfied by introducing PID controller.

$$K_D\Delta\dot{\alpha}+K_P\Delta\alpha+K_I\int dt=\dot{\alpha}_c \tag{33}$$

where K_D is the differential parameter, K_P the proportion parameter, and K_I the integral parameter. Second-order model for α_c is

$$\Omega\omega_n\dot{\alpha}_m+2\zeta_n\alpha_m+\omega_n^2\int\alpha_m dt=2\zeta_n\omega_n\alpha_c \tag{34}$$

where Ω is the amplification coefficient, ω_n the natural frequency, and ζ_n the damping coefficient. Structure of dynamic-inversion PID controller is shown in Fig. 14. By adjusting K_D, K_P, K_I, the controller will present a good robustness under the perturbation of aerodynamic parameters.

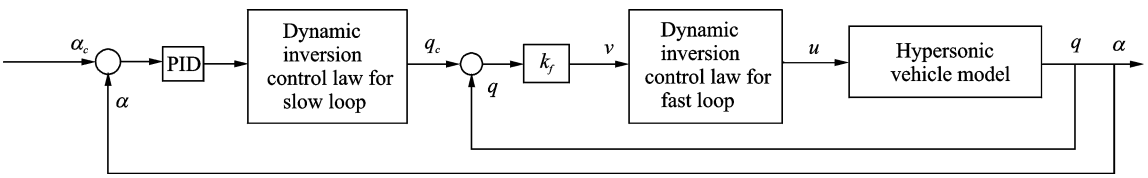

Fig. 14 Structure of dynamic-inversion PID controller

3.2.3 Simulation results

Dynamic-inversion controller without PID is firstly applied to the attitude control of the hypersonic vehicle. The initial condition is $V=150$ m/s, $H=3\ 620$ m, $\alpha=0°$, $q=0$ °/s. Simulation results without aerodynamic perturbations are shown in Figs. 15, 16.

The results show that dynamic-inversion controller without PID presents a good tracking performance in the premise of accurate vehicle modeling and no aerodynamic perturbations. Considering the severe uncertainties and nonlinearity, disturbances are added to test the robustness of dynamic-inversion controller: ±20% perturbations of m, S_w, c, C_L, C_{m_α}. The attack angle response is shown in Fig 17.

The results show that dynamic-inversion controller presents a bad tracking performance in the presence of disturbances. Big error is caused between the command signal and the response. Then, PID controller is combined with dynamic-inversion controller to test the robustness. K_D, K_P, K_I are chosen

$$K_p=2, K_I=0.5, K_D=4$$

Figs. 18—20 show the simulation results

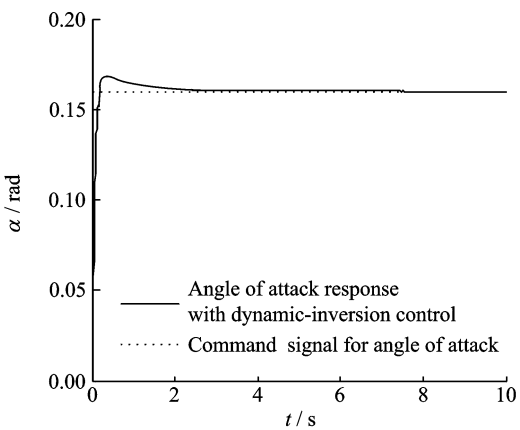

Fig. 15 Attack angle response without perturbation

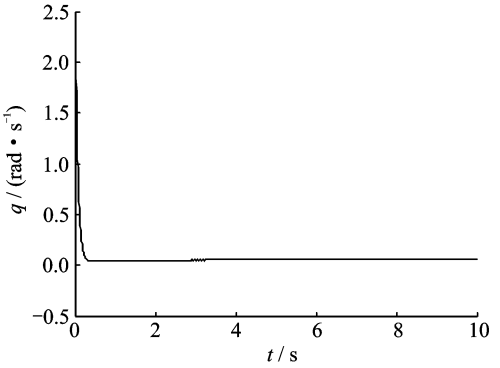

Fig. 16 Pitch rate response without perturbation

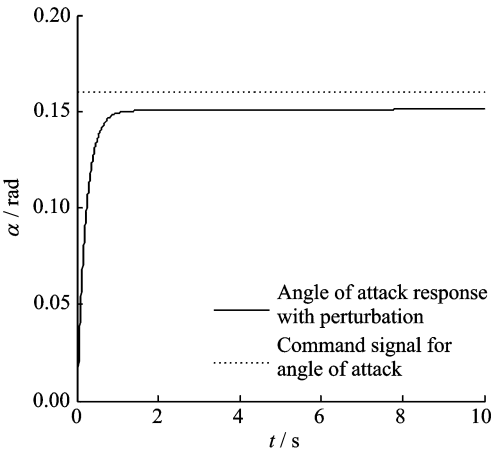

Fig. 17 Attack angle response with perturbation

controlled by dynamic-inversion PID controller in the presence of disturbances: ± 20% perturbations of $m, S_w, c, C_L, C_{m_\alpha}$.

Figs. 19, 20 show that dynamic-inversion PID controller presents a good tracking performance as well as a good robustness. No big error is caused between the command signal and the response. Therefore, the dynamic-inversion PID controller designed in this section is proved to be the effective nonlinear SAS for the hypersonic vehicle. The SAS is capable of tracking accurately and rapidly without big error.

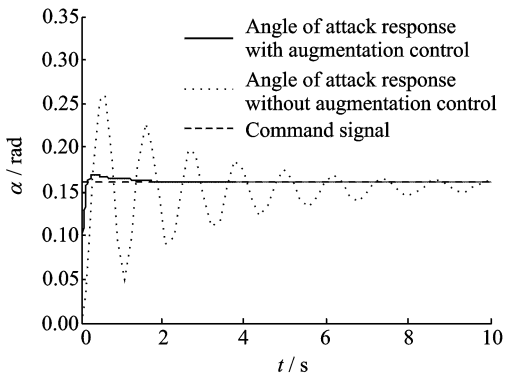

Fig. 18 Comparison of attack angle responses

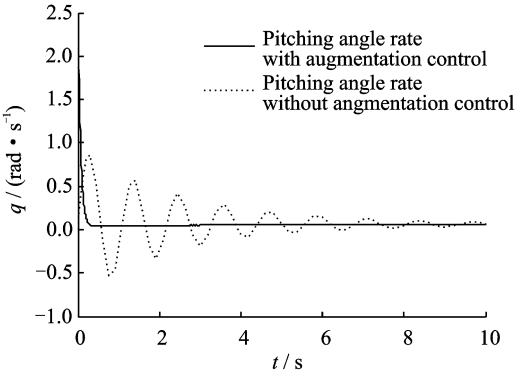

Fig. 19 Comparison of pitch rate responses

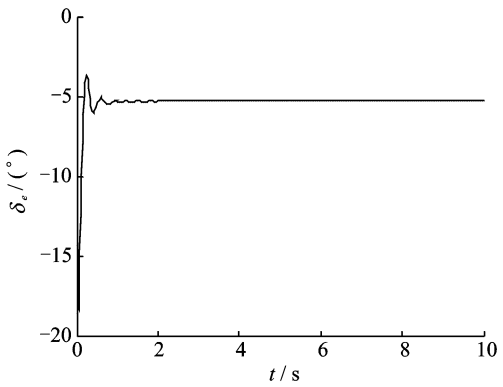

Fig. 20 Elevator deflection response

4 Conclusions

The contradiction between stability and maneuverability of the hypersonic vehicle is solved in this paper. In the first step, after analyzing the quantitative relationship between static stability and maneuverability, the specific static stability is obtained on the premise of good maneuverability in hypersonic flight. Second, aerodynamic parameters are adjusted properly based on the studied quantitative relationship between static stability and aerodynamic parameters to achieve the specific static stability, which will consequently lead to the vehicle instability in subsonic flight. Then the SAS is designed to ensure the stability in subsonic flight. Finally, the simulation results show the effectiveness of the proposed nonlinear SAS. It is verified that with various uncertainties, better performances and robustness is achieved rather than the linear SAS.

Acknowledgments

This work was supported in part by the National Natural Science Foundation of China (Nos. 61673209, 61741313), the Funding of Jiangsu Innovation Program for Graduate Education (No. CXZZ13_0170); the Funding for Outstanding Doctoral Dissertation in NUAA (No. BCXJ13-06); the Jiangsu Six Peak of Talents Program (No. KTHY-027); the Funding of China Launch Vehicle Technology Innovation Program of University and Institute (No. CALT 201503); and the Aeronautical Science Foundation (No. 2016ZA52009).

References:

[1] LUO X, LI J. Fuzzy dynamic characteristic model based attitude control of hypersonic vehicle in gliding phase[J]. Sci China Inf Sci, 2011, 54(3): 448-459.

[2] FAN M, CAO W, FANG X J. Prediction of hypersonic boundary layer transition with variable specific heat on plane flow[J]. Sci China-Phys Mech Astron, 2011, 54(11): 2064-2070.

[3] DONG M, LI X L. Problems of the conventional BL model as applied to super/hypersonic turbulent boundary layers and its improvements[J]. Sci China-Phys Mech Astron, 2011, 54(10):1889-1898.

[4] CHEN X Q, HOU Z X, LIU J X, et al. Phugoid dynamic characteristic of hypersonic gliding vehicles [J]. Sci China Inf Sci, 2011,54(3):542-550.

[5] GAO Y Y, HE F, SHEN M Y. Aerodynamic airfoil design using the Euler equations based on the dynamic evolution method and the control theory[J]. Sci China-Phys Mech Astron, 2011,54(4): 697-702.

[6] XU M L, CHEN K J, LIU L H, et al. Quasi-equilibrium glide adaptive guidance for hypersonic vehicles[J]. Sci China Tech Sci, 2012, 55(3): 856-866.

[7] LI X D, XIAN B, DIAO C, et al. Output feedback control of hypersonic vehicles based on neural network and high gain observer[J]. Sci China Inf Sci, 2011, 54(3): 429-447.

[8] SHIN Y, CALISE A J, JOHNSON M. Adaptive control of advanced fighter aircraft in nonlinear fight regimes[J]. Journal of Guidance, Control, and Dynamics, 2008, 31(5): 1464-1477.

[9] PEREZ R E, LIU H T, BEHDINAN K. Relaxed static stability aircraft design via longitudinal control-configured MDO methodology[J]. Canadian Aeronautics and Space Journal, 2006, 52(1):1-14.

[10] ZHOU Kun, WANG Lixin. Handling qualities assessment of short period mode for fly-by-wire passenger airliner with relaxed static stability design [J]. Acta Aeronautica et Astronautica Sinica, 2012, 33(9):1606-1615.

[11] ASHKENAS I L, KLYDE D H. Tailess aircraft performance improvements with relaxed static stability: NASA-CR-181806[R]. USA: NASA, 1989.

[12] CHEN Chuang. Research on large civil aircraft based on active control technology[D]. Shanghai: Shanghai Jiao Tong University, 2013.

[13] BLIGHT J D, GANGSAAS D, RICHARDSON T M. Control law synthesis for an airplane with relaxed static stability[J]. Journal of Guidance, Control and Dynamics, 1986, 9(5): 546-554.

[14] KRISHNASWAMY K, PAPAGEORGIOU G. Analysis of aircraft pitch axis stability augmentation system using sum of squares optimization[C]//Proceedings of the American Control Conference. USA: IEEE, 2005.

[15] UR REHMAN O, PETERSEN I R, FIDAN B. Feedback linearization-based robust nonlinear control design for hypersonic fight vehicles[J]. Proceedings of the Institution of Mechanical Engineers, Part I: Journal of Systems and Control Engineering, 2013, 227(1):3-11.

[16] STEINHAUSER R, LOOYE G. Design and evaluation of control laws for the X-31A with reduced vertical tail: AIAA 2004-5031[R]. USA: AIAA 2004.

[17] STEWART P, GLADWIN D. Multi-objective evolutionary-fuzzy augmented flight control for an F16 aircraft[J]. Proceedings of the Institution of Mechanical Engineers, Part G: Journal of Aerospace Engineering, 2010, 224(3): 293-309.

[18] MOGHADDAM M M, MOOSAVI D F. Robust maneuvering control design of an aircraft via dynamic inversion and μ-synthesis[J]. Proc I MechE, Part G: J Aerospace Engineering, 2005, 219(1): 11-18.

[19] XU H J, LEUNG P, MIRMIRANI M, et al. Adaptive sliding mode control design for a hypersonic flight vehicle[J]. Journal of Guidance, Control, and Dynamics,2004, 27(5):829-838.

[20] WANGM Q, STENGLE R F. Robust nonlinear control of a hypersonic aircraft[J]. Journal of Guidance, Control, and Dynamics, 2000, 23(1): 577-585.

[21] FIORENTINI L, SERRANI A, BOLENDER M A, et al. Nonlinear robust adaptive control of flexible air-breathing hypersonic vehicles [J]. Journal of Guidance, Control, and Dynamics, 2009, 32(2): 502-417.

[22] MOOJ E. Simple adaptive bank-reversal control of a winged re-entry vehicle: AIAA, 2004-4869 [R].

USA: AIAA, 2004.

[23] JOHNSON E N, CALISE A J, EI-SHIRBINY H A. Feedback linwarization with neural network augmentation applied to X-33 attitude control: AIAA, 2000-4157[R]. USA: AIAA, 2000.

[24] LIANG Bingbing, JIANG Ju, ZHEN Ziyang, et al. Improved shuffled frog leaping algorithm optimizing integral separated PID control for unmanned hypersonic vehicle[J]. Transactions of Nanjing University of Aeronautics and Astronautics , 2015, 32(1): 110-114.

[25] FIORENTINI L, SERRANI A. Nonlinear robust adaptive control of flexible air-breathing hypersonic vehicles[J]. Journal of Guidance, Control, and Dynamics,2009, 32(2): 401-416.

[26] BOLENDER M A, DOMAN D B. Non-linear longitudinal dynamical model of an hypersonic air-breathing vehicle[J]. J Spacecraft Rockets, 2007, 44(2): 374-387.

[27] CLARK A, WU C, MIRMIRANI M, et al. Development of an airframe-propulsion integrated generic hypersonic vehicle mode: AIAA 2005-6257 [R]. USA: AIAA, 2005.

[28] KESHMIRI S, COLGREN R. Six-DOF modeling and simulation of a generic hypersonic vehicle: AIAA 2006-6694[R]. USA: AIAA, 2006.

[29] KRENER A J. On the equivalence of control systems and linearizations of nonlinear systems[J]. SIAM Journal of Control and Optimization, 1973, 11(4): 670-676.

[30] TOMCZYK A. Aircraft maneuverability improvement by direct lift control system application[J]. Aerospace Science and Technology, 2005, 9(8): 692-700.

[31] GOMAN M G. Evaluation of aircraft performance and maneuverability by computation of attainable equilibrium sets[J]. Journal of Guidance, Control, and Dynamics, 2008, 31(2): 329-339.

Ms. **Wu Yushan** received her B. S. and M. S. degrees in automation from Nanjing University of Aeronautics and Astronautics (NUAA), Nanjing, China, in 2013 and 2016, respectively. From 2016 to present, she has been with the Chengdu Aircraft Design & Research Institute, where he is currently an engineer. Her research has focused on aircraft flight control.

Prof. **Jiang Ju** received his B. S. and M. S. degrees in automation from Beijing University of Aeronautics and Astronautics (BUAA), Beijing, China, in 1985 and 1988, and his Ph. D. degree in control from University of Waterloo, Canada, respectively. From 1988 to present, he has been with the Nanjing University of Aeronautics and Astronautics (NUAA), where he is currently a professor. His research has focused on aircraft flight control.

Dr. **Zhen Ziyang** received his M. S. and Ph. D. degrees in control from Nanjing University of Aeronautics and Astronautics (NUAA), Nanjing, China, in 2007 and 2010, respectively. From 2010 to present, she has been with the NUAA, where he is currently an associate professor. Her research has focused on flight control of carrier based aircrafts and hypersonic vehicles, preview control and adaptive control.

Dr. **Jiao Xin** received her M. S. and Ph. D. degrees in control from Nanjing University of Aeronautics and Astronautics (NUAA), Nanjing, China, in 2012 and 2016, respectively. Her research has focused on control engineering.

Mr. **Gu Chengfeng** received his B. S. and M. S. degrees in automation from Nanjing University of Aeronautics and Astronautics (NUAA), Nanjing, China, in 2013 and 2016, respectively. His research has focused on control engineering.

(Executive Editor: Zhang Bei)